Molecular Crystals and Liquid Crystals Science and Technology. Section A. Molecular Crystals and Liquid Crystals

Publication details, including instructions for authors and subscription information:
http://www.tandfonline.com/loi/gmcl19

# Vibronic Structure of Frenkel and Charge-Transfer Excitons in PTCDA

M. H. Hennessy [a], R. A. Pascal Jr. [a] & Z. G. Soos [a]

[a] Department of Chemistry, Princeton University, Princeton, NJ, 08544, USA

Version of record first published: 24 Sep 2006

To cite this article: M. H. Hennessy, R. A. Pascal Jr. & Z. G. Soos (2001): Vibronic Structure of Frenkel and Charge-Transfer Excitons in PTCDA, Molecular Crystals and Liquid Crystals Science and Technology. Section A. Molecular Crystals and Liquid Crystals, 355:1, 41-63

To link to this article: http://dx.doi.org/10.1080/10587250108023653

*Mol. Cryst. Liq. Cryst.*, Vol. 355, pp. 41-63
Reprints available directly from the publisher
Photocopying permitted by license only





# Vibronic Structure of Frenkel and Charge-Transfer Excitons in PTCDA

M.H. HENNESSY, R.A. PASCAL JR. and Z.G. SOOS*

*Department of Chemistry, Princeton University, Princeton, NJ 08544 USA*

*(Received December 04, 1999; In final form March 10, 2000)*

Perylenetetracarboxylic dianhydride (PTCDA) is ideal for applying molecular exciton theory to the evolution of molecular to solid-state excitations. The spectra of crystalline films and superlattices differ from solution due to the formation of uniform stacks. PTCDA shows mixing of nearly degenerate Frenkel and charge-transfer (CT) excited states and strong coupling to an out-of-phase C-C, C=C intramolecular stretch that corresponds to the effective conjugation coordinate of polymers. Its structural, electronic and vibrational simplicity can be modeled by a diatomic stack rather than a three-dimensional molecular lattice. Uniform stacks are realizations of Holstein models and provide the first example of vibronic coupling to mixed Frenkel-CT excitons. CT participation is analogous to polaron pairs on adjacent polymer chains, while Frenkel excitons are related to polyene and intrachain excitations. Calculated molecular parameters are consistent with spectroscopic values. Absorption processes show little dispersion and increased vibronic width; fluorescence is phonon-assisted and shifts to lower energy with increasing stack length; substituted perylenes form stacks with different overlaps and spectra. Localized and extended PTCDA states illustrate both interchain interactions in polymer films where single-crystal resolution is lacking and organic molecular crystals with more extensive and complicated solid-state contributions.

*Keywords:* exciton-vibrational models; absorption and fluorescence; molecular computations; vibronic structure

## 1. INTRODUCTION

Organic crystals illustrate a variety of intermolecular interactions.[1,2] Molecular exciton theory starts with isolated molecules and treats solid-state perturbations that shift and split molecular excitations. Frenkel excitons are delocalized molecular excited states that dominate the absorption and emission of organic crystals; they couple to both molecular and lattice vibrations. Charge-transfer (CT) excitons consist of nearby ion-pairs. They appear in electroabsorption of Frenkel sys-

* Corresponding Author.

tems[3] and are the lowest optical excitation in donor-acceptor and ion-radical crystals.[4] Although artificial, separate treatment of Frenkel and CT excitons reflects the difficulties of describing overlapping bands in extended systems. Excited-state mixing is necessary to account for charge generation, photoconductivity or transport. We describe in this paper mixed Frenkel-CT excitons in perylenetetracarboxylic dianhydride (PTCDA), whose extensive spectroscopy[5] and structural, electronic and vibrational simplicity make it an ideal molecular crystal to model.[6]

Conjugated polymers resemble molecular crystals in having interchain interactions at van der Waals separations. The electronic structure of single chains has been discussed from such contrasting perspectives as one-dimensional semiconductors, correlated oligomers, or distributions of segments.[7,8] Conjugated polymers have metallic conductivity on doping, large nonlinear optical susceptibilities, and applications as light-emitting diodes and optoelectronics. Except for polydiacetylene single crystals, conjugated polymers are amorphous and their morphology varies with preparation. The broad spectra of films hinder detailed modeling. Pristine polymers have even and odd-parity excitons;[9] solitons, polarons and bipolarons appear on doping.[10] Recent studies, both experimental and theoretical, have focused on interchain interactions. CT between adjacent strands generates polaron pairs[11] or excimers with indirect contributions to the photophysics.

PTCDA, sexithiophene[12] and other crystals with both molecular and extended states serve to bridge molecular crystals and conjugated polymers. Their molecular excitations and vibronic structure are analogous to the excited states of a single chain, while CT and intermolecular interactions correspond to interchain processes. Comparison of PTCDA spectra in dilute solution and crystalline films, for example, quantitatively identifies solid-state contributions to absorption and emission. The evolution of electronic structure from molecules or polymers to solids has great generality. Molecular systems have overlapping Frenkel and CT excitations, vibronic coupling to normal modes, and close neighbors in three dimensions. Although identified and catalogued,[1,2] these states and interactions are rarely amenable to quantitative modeling. We discuss in this paper why PTCDA is an exception.

PTCDA crystallizes in face-to-face stacks with uniform spacing below van der Waals contact.[5] Its electronic structure and photoconductivity are highly one dimensional. The lowest $\pi$-$\pi^*$ excitation is directly related to polyenes,[13] with strong vibrational coupling to a single mode, the effective conjugation coordinate of polymers.[14] These structural and electronic features are simpler than encountered in previously studied organic crystals such as anthracene and lead to one-dimensional theoretical models. Figure 1 summarizes[15] the evolution from

molecular to crystal states, as discussed in the following Sections. We apply exciton theory to the $\pi$-$\pi^*$ excitation, denoted $M^*$, with vibrational quanta $\hbar\omega$ and harmonic potential with displacement g and reorganization energy $\hbar\omega g^2$. We postulate a CT state at $2\Delta$ from $M^*(0,0)$ with different reorganization energy. Stack formation generates a Frenkel-exciton band, as sketched in Fig. 1, with crystal selection rules for absorption and emission. We neglect the CT bandwidth, focus on mixing with the nearly degenerate $M^*$ vibronics, and analyze PTCDA spectra to obtain mixed Frenkel-CT vibronics starting at $E_1$ in the k = 0 manifold.

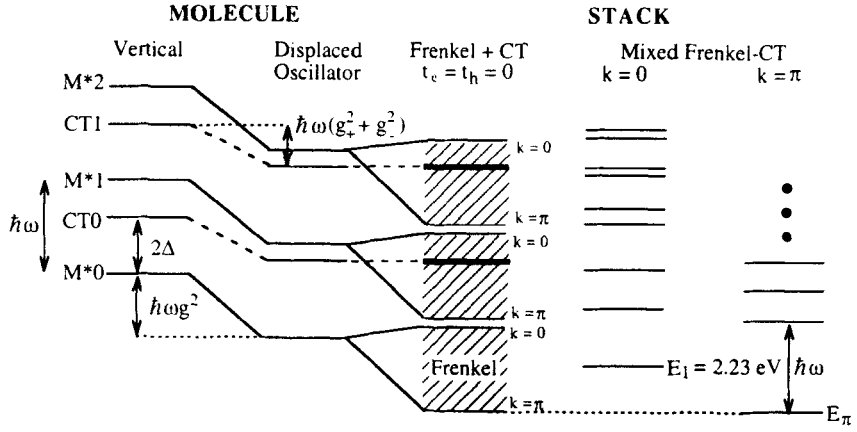


FIGURE 1 Molecular and CT excitations of PTCDA stacks. The $M^*$ energies are $-g^2$ + m in units of $\hbar\omega$; the $M^+M^-$ vibronics are $2\Delta - g_+^2 - g_-^2$ + m. The middle column has finite Frenkel bands and no CT width or Frenkel-CT mixing. The last two columns show mixed states, with $E_1$ = 2.23 eV lowest at k = 0 and phonon-assisted absorption at k = $\pi$

PTCDA shows the *minimum* information needed for treating mixed Frenkel-CT vibronics or nearly degenerate polaron pairs and excitons in conjugated polymers. A single coupled mode suffices at 0.10 eV resolution; $M^*$ is an eV below the next $\pi$-$\pi^*$ excitation; and CT contributes to $E_1$ rather than at higher energy. Solution and film spectra presented in Sections 2 and 3 lead to the parameters in Table I. The primary evidence for CT is the Stark shift for a static field normal to the PTCDA plane, since an ion pair $M^+M^-$ has the requisite polarizability along the stack. These unusually favorable circumstances are complemented by the extensive spectroscopy in crystalline films and superlattices.[5] Typical organic crystals have several coupled modes, each of which requires a displaced oscillator, in structures with several molecules per unit cell and more than one nearby Frenkel and CT state.

TABLE I PTCDA parameters for $H_{ex}$, Eq. (2) and $H_d$, Eq. (10)

| *Parameter* | *Role* | *Source or related quantity* |
|---|---|---|
| $\hbar\omega = 0.18$ eV | vibrational quantum | solution, ref. 19, and polyenes |
| $g = 0.84$ | excited-state displacement | 0.84 in $CH_2Cl_2$, ref. 19 |
| $J = 204$ meV | exciton hopping | transition dipoles, Eq. (15) |
| $\Delta = 121$ meV | CT position | adjustable, model |
| $\lvert t_e + t_h\rvert/2 = 62$ meV | Frenkel-CT mixing | adjustable, model |
| $(g_+ + g_-)/2 = 0.76$ | ionic displacement | adjustable, relaxation energies |
| $E_1 = 2.23$ eV | absorption origin | free |
| $\delta_S = 70$ meV | Stokes shift | solution, ref. 19, adjustable |

An evolution from molecular to crystal states occurs quite generally in organic crystals and interchain interactions in polymers, and detailed understanding of PTCDA photophysics transcends a single system. PTCDA provides the best evidence to date for the vibronic structure of mixed Frenkel-CT excitons, for the realization of a Holstein model and its generalization to CT excitations, and for internally consistent parameters that describe absorption and emission.[6,15] The following analysis of PTCDA stacks is nevertheless preliminary. Low-temperature studies on superlattices may require extensions, dielectric or transport properties remain to be included, and other perylenes with stacked structures have to considered. Higher resolution or time-resolved spectra may justify more comprehensive modeling.

## 2. PTCDA SPECTRA FROM MOLECULES TO STACKS

Substituted perylenes have strikingly similar absorption in solution.[16] The perylene core in Fig. 2a has twenty $\pi$-electrons and $D_{2h}$ symmetry. The frontier orbitals are odd under reflection in the xz plane, a general feature of rylenes from naphthalene to polyperinaphthalene.[13] Perylene or PTCDA has eight $\pi$-electrons in orbitals that are odd under xz reflection and have nodes at carbons on the x axis. The Hückel model for odd orbitals maps exactly[13] into octatetraene,

$$H_0 = \sum_{n=1,\sigma} -t_{n,n+1}(c^+_{n,\sigma}c_{n+1,\sigma} + c^+_{n+1,\sigma}c_{n,\sigma}) \qquad (1)$$

with n = 1,2,...,7. Each expanded site n in (1) is the odd linear combination of $sp^2$ carbons. The transfer integrals $t_{n,n+1}$ are related to partial single and double bonds, and are more uniform in rylenes[17] than in polyenes. Expanded sites reduce Coulomb interactions in the Pariser-Parr-Pople model for $\pi$-electrons, and

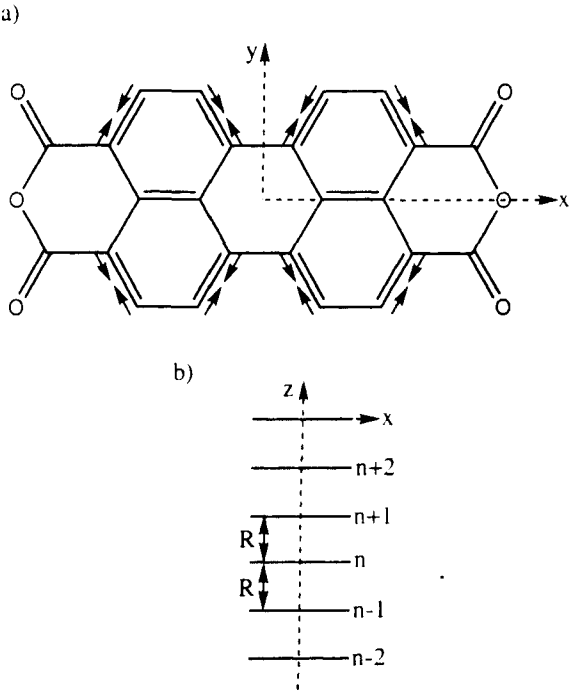


FIGURE 2 (a) PTCDA conjugation and principal axes; the coupled mode indicated schematically is the out-of-phase C-C and C=C stretches of the perylene periphery. (b) Idealized PTCDA stacks along **z**, with interplanar separation R = 3.38 Å and $\pi$-$\pi^*$ transition dipole along **x**

exact PPP solutions with standard parameters account well for both molecular and polymeric excitations.[18]

The intense $\pi$-$\pi^*$ transition of PTCDA is x-polarized and corresponds to the $1^1B_u$ excitation of octatetraene or conjugated polymers whose backbones have inversion symmetry. Expanded sites lower $1^1B_u$ by an eV compared to polyenes.[13] This reverses the order of $1^1B_u$ and $2^1A_g$, the lowest even-parity singlet. Perylenes have strong fluorescence from $S_1 = 1^1B_u$ that mirrors their absorption; the weak, anomalous emission of polyenes at cryogenic temperatures is from $S_1 = 2^1A_g$. The 1B/2A ordering of polyenes is an important manifestation of correlations[18] that bears directly on the photophysics of conjugated polymers.[9] Conjugated chains also have strong electron-phonon coupling.[10] The out-of-phase stretch of C=C and C-C bonds sketched in Fig. 2a interchanges single and double bonds and modulates the optical gap. It is the effective conjugation coordinate whose projection along $a_g$ modes appears in resonance Raman spectra.[9]

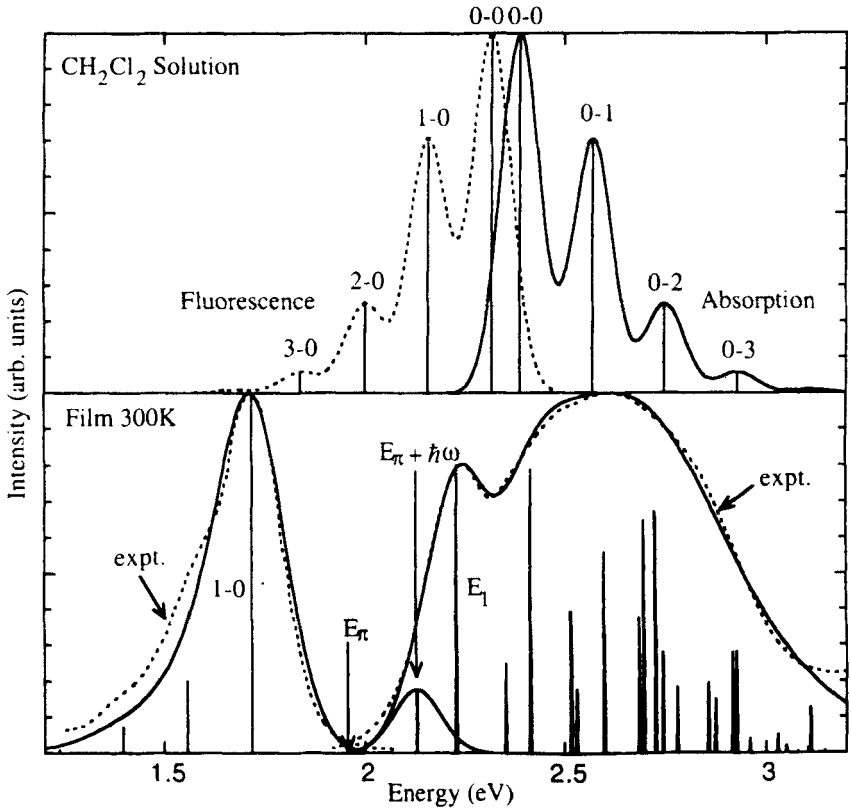


FIGURE 3 (a) PTCDA absorption and emission in methylene chloride, from ref. 19, fit to a displaced harmonic oscillator with $\hbar\omega = 0.18$ eV, $g = 0.84$, and Gaussian profiles; (b) PTCDA absorption and emission in thick films at 300 K, from ref. 24, with fits based on Table I and ref. 6. The top and bottom of the exciton band are $E_1$ and $E_\pi$, respectively

PTCDA absorption and fluorescence in methylene chloride[19] are shown in Fig. 3a. At 0.1 eV resolution, a progression in $\hbar\omega = 0.18$ eV is quantitative and gives displacement $g = 0.84$ that will be retained in stacks. The relative intensity of 0-p is $(g^{2p})/p!$ for displaced harmonic oscillators. The same 0.18 eV mode appears in polyenes and polyacetylene as well as rylenes and pyrenes. Polyenes[20] have larger $g \sim 1$ and slightly more intense 0–1 than 0–0. Expanded sites reduce g by $\sqrt{2}$, since the molecular excitation is delocalized over two conjugated strands. The fluorescence in Fig. 3a is similarly simple, with a small Stokes shift of 70 meV due to all other modes, the same $g = 0.84$, and smaller ground state spacing of 0.16 eV as also found in polyenes.[20] The fluorescence quantum yield of perylenes is typically over 50%. Solution spectra highlight the

molecular simplicity of PTCDA. Since the next allowed transition is almost an eV above $1^1B_u$ and there is one active mode, we effectively have a diatomic rather than a large conjugated molecule.

Molecular spectra are inputs in exciton theory. Eclipsed stacking is depicted in Fig. 2b for PTCDAs with orthogonal long (x) and stacking (z) axes. The molecules in the actual structure[21] are slipped by 1.19 and 1.05 Å along x and y, respectively, and the angle between x and z is 72°. Solid-state spectra of substituted perylenes[16] are empirically related to x,y offsets. We discuss the idealized eclipsed stack in Fig. 2b and defer refinements to Section 5.

Close contacts R = 3.38 Å along the stack, uniform spacing and coupling to a molecular vibration lead to a Holstein model[22] for Frenkel excitons,

$$H_{ex} = \sum_p \{J(a_p^+ a_{p+1} + a_{p+1}^+ a_p) + \hbar\omega g a_p^+ a_p (b_p^+ + b_p) + \hbar\omega b_p^+ b_p\}. \qquad (2)$$

The sum p is over molecules in the stack; $a_p^+$ creates a vertical $1^1B_u$ ($M^*$) excitation at the pth molecule and $J = \langle M^*M|H|MM^*\rangle$ describes nearest-neighbor hops along the stack; the boson operators $b_p^+$ create vibrational quanta; and the $M^*$ oscillator is displaced by g but retains the ground state frequency. Linear electron-vibration coupling and displaced harmonic oscillators are standard approximations for extended systems. The parameters g and $\hbar\omega$ follow directly from solution spectra. Since J is related to the $1^1B_u$ oscillator strength, we could argue that (2) contains no adjustable parameters. We have an exciton band 2Jcosk for g = 0, with wavevector $-\pi < k \leq \pi$ in the first Brillouin zone, and molecular excitations when J = 0. The relative magnitudes of g, J and $\hbar\omega$ govern the balance between excitation delocalization and localization.[23]

PTCDA stacks immediately rationalize[6] the absorption and emission changes in Fig. 3b; detailed fits are discussed in Section 3. Since $1^1B_u$ is x-polarized, adjacent transition dipoles repel and k = 0 is at the top of the band, $k = \pi$ at the bottom. The allowed crystal transition to k = 0 is broadened for antibonding J > 0. Reduced dispersion at k = 0 is suggested in Fig. 1 and modeled below with CT contributions in addition to (2). Emission from $k = \pi$ relates the large red shift in Fig. 3b to the width of the Frenkel band. The transition is dipole forbidden, consistent with ~ 100-fold lower quantum efficiency for film fluorescence, and becomes allowed on creating a $q = \pi$ phonon in the ground state. The main peak at 1.71 eV is accordingly assigned as the 1–0 transition. Similarly, phonon-assisted absorption is allowed at $k = \pi$ and explains the sharp peak at 2.11 eV in the fluorescence excitation spectrum;[24] this transition is shown separately in Fig. 3b.

PTCDA stacking is responsible for all changes between Fig. 3a and b. Such precise data is not available for interchain interactions in conjugated polymers. In

typical organic crystals, by contrast, detailed modeling is hindered by more extensive solid-state modifications. We will need to generalize (2) to include a CT state in order to model k = 0 processes such as absorption and electroabsorption. CT is less important for emission and is neglected at present. We apply (2) to the emission of thick films with infinite stacks, superlattices with short stacks, and dimers in solution.



## 3. MOLECULAR EXCITON ANALYSIS OF PTCDA STACKS

Extensive PTCDA spectra in crystalline films, superlattices and solution present major challenges as well as opportunities for decisive interpretation. Our discussion is broadly applicable to molecular crystals and conjugated polymers. We address several different issues. The first is the vibronic structure of Frenkel excitons: we apply variational and numerical methods to (2). The second is Frenkel-CT mixing in extended chains and its dependence on wavevector and intermolecular overlap: we extend linear coupling to CT excitons and argue for large effective mass at k = 0, which gives the crucial dimer approximation. The third is direct solution of the Frenkel-phonon-CT dimer and its application to k = 0 spectra. We conclude with independent calculations of the parameters in Table I.

### 3.1 Vibronic structure of Frenkel excitons

The Holstein model (2) has primarily been applied to polaron or exciton transport and to the possibility of self-trapping transitions. A host of theoretical methods have delineated various regimes of g, J and $\hbar\omega$, but there is no general solution. Recent studies discuss the convergence of numerical solutions[25] with increasing oligomer length or the properties of refined trial functions[26] with both local and nonlocal variational parameters.

We denote a $\pi$-$\pi^*$ excitation at site p as $|M_p^*\rangle$ and introduce trial functions

$$|M_p^*\rangle = a_p^+ \left[ \exp\left( \sum_j -\frac{1}{2}\lambda_j^2 + \lambda_{p-j} b_j^+ \right) \right] |0,0\rangle \qquad (3)$$

for sites p = 1,2,... N. The vacuum state $|0,0\rangle$ is a product function for a stack with all molecules in the ground electronic and vibrational state. The $\lambda_j$ are displacements along the coupled mode that are found variationally. The trial function (3) is normalized for arbitrary $\lambda_j$ and has a phonon cloud centered at p. Cyclic boundary conditions lead to Frenkel excitons

$$|F,k\rangle = N^{-1/2} \sum_p |M_p{}^*\rangle \exp(ikp) \tag{4}$$

with k = 0, ±2π/N, ..., π in the first Brillouin zone. The functions (4) are normalized because the electronic excitation is confined to a single site. The expectation value of (2) is[6]

$$E_k = \langle F,k|H_{ex}|F,k\rangle = 2JS_k \cos k - 2g\hbar\omega\lambda_0(k) + \hbar\omega \sum_j \lambda_j(k)^2 \tag{5}$$

where $S_k = \exp[-\Sigma_j(\lambda_j - \lambda_{j+1})^2/2]$ is the Franck-Condon overlap for electronic excitation at adjacent sites and the k-dependence of the displacements is explicitly shown.

The minimization of $E_k$ with respect to $\lambda_j$ was originally carried out by Merrifield[27] for a trial function with complex variational parameters. Real $\lambda_j$ give the same result at the band edges[6] and were independently proposed for linear aggregates.[28] Linear coupling and harmonic oscillators in (2) ensure the sum rule,

$$g = \sum_j \lambda_j(k). \tag{6}$$

The total displacement associated with an exciton is conserved. The J = 0 result for noninteracting molecules is $\lambda_{p\text{-}j} = g\delta_{pj}$ and displacements confined to $M_p{}^*$ in (3). We still have $g = \lambda_0$ at $k = \pm\pi/2$ for finite J because these degenerate states have nodes at every other site. At k = 0, delocalization is antibonding for J > 0 and the variational solution minimizes $E_0$ by reducing $S_0$; we find $\lambda_0(0) > g$ and displacements with alternating signs in (6). The lattice strain, which is the $\lambda_j{}^2$ sum in (5), exceeds the molecular reorganization energy, $g^2$. At $k = \pi$, where delocalization is stabilizing, we have $\lambda_0(\pi) < g$ and displacements with the same sign in (6) that increase $S_\pi$ and decrease the lattice strain. These cases correspond to nonbonding, antibonding and bonding interactions, respectively.

The trial functions (4) are not Born-Oppenheimer states, since the displacement of the coupled mode depends on the electronic excitation, and nonadiabatic states are a basic feature of variational methods. Comparisons with numerical solutions show good agreement at the bottom of the band that extends to vibronic intensities, while energies but not intensities are adequate at the top.[28,29] The fluorescence fit in Fig. 3b is based[15] on the variational solution and parameters in Table I, especially J = 204 meV. The ansatz (3) can readily be applied to stacks with open boundary conditions. The superlattice fluorescence in Section 4 is based on direct solution of (2) for finite stacks; variational results are virtually the same.[29] The antibonding nature of J > 0 at the top of the band appears as reduced dispersion in direct simulations[25] as well as increased absorption width of PTCDA films.

### 3.2 Frenkel-CT mixing

We define $|M_p^+\rangle$ and $|M_q^-\rangle$ as the ground state of a cation and anion radical, respectively, at site p and q of the stack. Functions such as (5) with ionic displacements along the coupled mode can be defined in general. The electron-hole symmetry of polyenes and the infrared active vibrations of doped polyacetylene suggest displacements for ions along the same coupled mode. We simply take $g_+ = g_- < g$ for ionic displacements relative to the PTCDA ground state and relate them to relaxation energies in Section 3.4. The functions $|M^+\rangle$ and $|M\rangle$ are even under inversion, while $|M^-\rangle$ and $|M^*\rangle$ are odd. The overlap $\langle M^+M^-|MM\rangle$ vanishes by symmetry for eclipsed PTCDAs.

We consider CT singlets of adjacent ion pairs with $|p - q| = 1$ and write

$$|CT\pm, k\rangle = (2N)^{-1/2} \sum_p \{|M_p^+ M_{p+1}^-\rangle \pm |M_p^- M_{p+1}^+\rangle\} \exp[ik(p + 1/2)]. \quad (7)$$

Each ion pair in (7) represents an $(\alpha\beta - \beta\alpha)/\sqrt{2}$ linear combination. Frenkel-CT mixing involves electron and hole transfer

$$t_h = \langle M_p M_{p+1}^* | H | M_p^+ M_{p+1}^- \rangle / \sqrt{2}, \quad t_e = \langle M_p^* M_{p+1} | H | M_p^+ M_{p+1}^- \rangle / \sqrt{2} \quad (8)$$

that require intermolecular overlap. PTCDA has high mobility for holes. These electronic integrals describe Frenkel-CT mixing in stacks with cyclic boundary conditions,[6]

$$\langle F, k | H | CT\pm, k' \rangle = \delta_{kk'} (t_h \pm t_e)[\exp(ik/2) \pm \exp(-ik/2)]. \quad (9)$$

The $k = k'$ restriction follows from translational symmetry and mixing at $k = 0, \pi$ is restricted to $|CT\pm\rangle$, respectively. Its strength depends on the relative signs of the transfer integrals (8) and the energy difference $2\Delta$ between CT and $1\,^1B_u$.

As sketched in Fig. 1, CT bands are assumed to have negligible width. Mixing at $k = 0$ further reduces the dispersion or increases the effective mass. This is the physical basis for approximating $k = 0$ processes by a dimer whose electronic and vibrational basis can readily be handled. Linear coupling to two or more electronic excitations, on the contrary, is intractable in extended systems even in the approximation of displaced harmonic oscillators.

### 3.3 The exciton-phonon-CT dimer

The dimer approximation for mixed states at $k = 0$ rests on dispersionless CT bands in organic crystals and vibronic flattening at the top of Holstein bands. We have four electronic states, $|r\rangle = |M^*M\rangle$, $|MM^*\rangle$, $|M^+M^-\rangle$ and $|M^-M^+\rangle$. Each molecule has a displaced harmonic potential in the excited state. The notation $|r,mn\rangle$

indicates m quanta $\hbar\omega$ in the first molecule and n in the second. The exciton-phonon-CT dimer is[6]

$$H_d = \sum_{r,s} h_{rs} a_r^+ a_s + \hbar\omega \sum_r a_r^+ a_r \Lambda_r + \hbar\omega(b_1^+ b_1 + b_2^+ b_2)$$
$$\Lambda_r \equiv g_{1r}(b_1^+ + b_1) + g_{2r}(b_2^+ + b_2) \tag{10}$$

with $h_{11} = h_{22} = 0$ for the M*, $h_{33} = h_{44} = 2\Delta$ for $M^+M^-$, $h_{12} = J$ for exciton hopping, $h_{13} = h_{24} = t_h\sqrt{2}$, $h_{14} = h_{23} = t_e\sqrt{2}$, and $h_{34} = 0$ for a two-electron transfer. The coupling constants $g_{1r}$, $g_{2r}$ are (g,0), (0,g) for r = 1,2 and ($g_+$,$g_-$), ($g_-g_+$) for r = 3,4. The generalization of (2) to displacements at adjacent sites for ion-pairs is natural and can readily be stated, if not solved, for infinite stacks.

As in polaron problems, we consider the subspace of $H_d$ with one electronic excitation, $\Sigma_r n_r = 1$. Transformation to displaced oscillators gives the molecular vibronics in Fig. 1,

$$\varepsilon_{rmn}/\hbar\omega = h_{rr} - g_{1r}^2 - g_{2r}^2 + m + n \tag{11}$$

with m,n = 0,1,2,... The diagonal energies (11) are exact in the absence of excitation transfer (J = 0) or Frenkel-CT mixing ($t_e = t_h = 0$), and the static limit holds in extended systems. The off-diagonal elements $r \neq s$ are

$$\langle r, m'n'|H_d|s, mn\rangle = h_{rs} F_{m'm}(g_{1s} - g_{1r}) F_{n'n}(g_{2s} - g_{2r}) \tag{12}$$

where the $F_{n'n}(g)$ are Franck-Condon overlaps that are known analytically for harmonic oscillators.

Four states $|r\rangle$ and two oscillators with p = m+n quanta generate 4(p+1) basis functions $|r,mn\rangle$. We have conveniently small $H_d$ matrices to solve, with p up to $p_{max} \sim 10$, for the 5 $\hbar\omega \sim 0.9$ eV interval spanned in absorption. Transitions from the $|MM00\rangle$ ground state are confined to low-energy states of $H_d$ for displacements up to $g \sim 1$, and the vibrational vacuum is sufficient when $\hbar\omega >> kT$. The expansion

$$|q\rangle = \sum_{rmn} c_{rmn,q} |r, mn\rangle \tag{13}$$

emphasizes the nonadiabatic nature of the $H_d$ eigenstates, with different potential for every r. The eigenvalues and eigenstates suffice for the relative intensities of all transitions in the Condon approximation.

The calculated absorption in Fig. 3b is based on $H_d$, the parameters in Table I, and Gaussian profiles with energy-dependent broadening.[6] The stick spectra are dipole transitions starting at $E_1$. The vibronics in $\hbar\omega$ are greatly modified by Frenkel-CT mixing. The extension of (10) to larger oligomers or to molecules with several coupled modes is straightforward[29] and the rapidly increasing dimensions of the basis can be estimated in advance. Oligomers produce denser

spectra that differ in detail from the dimer transitions in Fig. 3b, but this requires higher resolution.

### 3.4 Molecular parameters

Early applications of excitons to organic crystals emphasized symmetry and relied on empirical parameters. Modern computations often provide independent estimates, although *ab initio* crystal parameters are not yet available. Intermolecular overlaps or interactions are naturally harder to treat than molecular properties that, especially for the ground state, can be computed at many levels. The relative energies of CT and molecular energies have the additional challenge of finding small, ~ 100 meV differences between ~ eV quantities.

The 6–31G(d) basis[30] has proven to be complete enough for reliable molecular geometry, but small enough for *ab initio* treatment of molecules as large as PTCDA. We used the Gaussian 94 program package (Gaussian 94, Revision D.4, Gaussian, Inc., Pittsburgh, Pennsylvania, 1995) with its built-in default thresholds for wavefunction and gradient convergence for geometry optimization, and tighter thresholds for single point calculations. We optimized[15] the perylene and PTCDA ground states using the B3LYP hybrid density-functional theory[31] and found the vertical excitations to the lowest triplet, denoted $^3$M, and to the ground states of $M^+$ and $M^-$. We optimized the excited states to find adiabatic excitations. The differences are the relaxation energies in Table 2. For $M^*$, we found[15] the Hartree-Fock ground state in the 6–31G(d) basis, the vertical excitation with configuration interaction for all singles, and relaxed $M^*$ using CIS/6–31G(d). The $t_h$ and $t_e$ entries in Table II are, respectively, half of the HOMO-HOMO and LUMO-LUMO splitting found in B3LYP for a PTCDA dimer at 3.38 Å and offsets of 1.19 and 1.05 Å along the long and short axis taken from the crystal structure.

TABLE II Molecular calculations of PTCDA and Perylene parameters

| | | *PTCDA* | *Perylene* |
|---|---|---|---|
| Relaxation energy (meV) | Cation radical, $M^+$ | 72 | 73 |
| | Anion radical, $M^-$ | 127 | 87 |
| | Triplet, $^3$M | 242 | 303 |
| | Singlet, $M^*$ | 323 | 353 |
| Tranfer integral (meV) | HOMO-HOMO, $t_h$ | 28 | |
| | LUMO-LUMO, $t_e$ | 07 | |

Hückel theory relates the HOMO and LUMO of alternant hydrocarbons such as perylene. Equal relaxation is predicted for $M^+$ on removing an electron from the HOMO and for $M^-$ on adding one to the LUMO. This explains the relaxation of perylene ions. The $M^*$ and $^3M$ relaxation, also equal, are the sum of the radical ions. Although PTCDA retains the perylene $\pi$-system, the inductive effects of sidegroups suggest different $M^+$, $M^-$ relaxation. The $M^*$ and $^3M$ relaxation are comparable and larger than the sum of the radical ions. Table II has several implications for our model. In Fig. 3a, $g^2\hbar\omega \sim 120$ meV is the relaxation along the coupled mode and the 70 meV Stokes shift is an estimate for other modes and the solvent. We have a simple and sensible starting point for the ~ 100 meV difference between the calculated and solution relaxation of $M^*$. Moreover, comparable $M^+$, $M^-$ relaxation suggests $g_+ \sim g_- \sim g/\sqrt{2}$, instead of the larger coupling we guessed for the anion.

Optimized excited states give displacements along the coupled mode and other changes of bond lengths and angles. All excited states in Table II have longer double bonds and shorter single bonds on the periphery in Fig. 2a and small changes along the x axis, consistent with the effective conjugation coordinate and an xz nodal plane for the Hückel HOMO and LUMO. The $M^*$ or $^3M$ changes along the periphery are about twice the $M^+$or $M^-$ displacements. Other changes of bond lengths and angles tend to be small. More quantitative normal mode analysis is straightforward.

Strong $\pi$-$\pi^*$ transitions have oscillators strengths $f = \Delta E\mu^2 \sim 1$, where $\mu$ is the transition dipole and $\Delta E$ is the excitation energy. Exact Pariser-Parr-Pople results are currently limited to 16 $\pi$-electrons,[32] but the 20 electrons of perylene or PTCDA are related to a modified octatetraene with expanded sites. The molecular transition dipole is a sum

$$\langle M|\mu|M^*\rangle = e\sum_{n\sigma} x_n\langle M|(c^+_{n\sigma}c_{n\sigma} - 1)|M^*\rangle \equiv e\sum_n x_n\langle M|q_n|M^*\rangle \qquad (14)$$

over atomic moment; $x_n$ is a distance along the long axis relative to an arbitrary origin and $q_n$ measures $\pi$-electron charge. The same integrals appear in J,

$$J = \langle M^*M|H|MM^*\rangle = \sum_{n\in 1, m\in 2} e^2R^{-1}_{nm}\langle M|q_n|M^*\rangle\langle M^*|q_m|M\rangle \qquad (15)$$

with sums over conjugated sites n,m of adjacent PTCDAs separated by $R_{nm}$. J is closely related to resonant transfer or dispersion forces[33] and does not require intermolecular overlap. Atomic transition moments reduce J by an order of magnitude from point dipoles. Similarly, the electrostatic (Madelung) energies of ion-radical salts require atomic charges $\rho_i$, as used below for the dipole of $|M^+M^-\rangle$, and fine-structure constants are given by atomic spin densities.[4]

The PPP result with extended sites is $\mu = 7.92$ D for (13) and $\Delta E = 3.07$ eV for the $\pi$-$\pi^*$ transition of perylene, whose experimental 0–0 of 2.86 eV is higher than PTCDA's 2.40 eV. We obtain $f = \Delta E\mu^2 = 0.73$ and $J = 190$ meV. The CIS/6–31G(d) calculation overestimates $\Delta E$ by an eV and gives $f = 0.78$ and 1.11, respectively, for perylene and PTCDA. Hückel theory, which is known to overestimate $\mu$, gives $J = 490$ meV for eclipsed perylenes at $R = 3.38$ Å. These estimates support the fitted $J = 204$ meV in Table I.

## 4. ELECTROABSORPTION, SUPERLATTICES AND SOLUTION SPECTRA

The discussion so far has focused on Fig. 3 and spectral changes due to PTCDA stacks in thick films. We now turn to other spectra and finite stacks. The polarization of light normal to well-developed (010) face of small single crystals can be varied from almost in the PTCDA plane to almost normal to it. The entire $\pi$-$\pi^*$ spectrum in Fig. 4 is in-plane polarized.[6] Almost isotropic absorption is expected in the xy plane for stacks whose long axes subtend a 72° angle. There is negligible CT in the ground state, in contrast to Mulliken complexes. Frenkel-CT mixing (8) involves excited states: all CT intensity is borrowed from $M^*$ ($1^1B_u$) and is consequently x-polarized. In the same way, excited-state mixing in conjugated polymers is compatible with transitions polarized along the backbone to polaron states on adjacent chains.[11] The mechanism is general and expected, but its realization and quantitative modeling in PTCDA is rare.

Electroabsorption (EA) spectra are the principal evidence for CT in PTCDA[5] as well as other organic crystals.[3] The change of absorption, $I(x,F) - I(x)$, in a static electric field F is particularly sensitive to polar states. The Stark shift[34] of the 2.23 eV line, the "thumb" in Fig. 3b, is nearly the same for F along the stack ($F_z$) or in the molecular plane ($F_\perp$). The shift $\Delta E = \Delta\alpha F^2/2$ gives the polarizability change between the ground and excited state.[6] As usual, the latter is more polarizable. We have $\Delta\alpha_\perp = 280$ Å$^3$ for $F_\perp$, which is due to delocalized $\pi$-electrons and is a molecular problem. The $F_z$ result, $\Delta\alpha_z = 320$ Å$^3$, far exceeds the polarizability and is primarily associated with CT. Although perfect molecular and CT separation is limited to eclipsed stacks, PTCDA is again close to ideal.

The $F_z$ shift associated with CT has a major role in fixing $2\Delta$ and $t_e = t_h$ in Table I. The dipole of the CT state $|M^+M^-\rangle$ in (7) is along z,

$$\mu_{CT} = eR \sum_{i\in M^+, j\in M^-} \rho_i \rho_j Z_{ij} \qquad (16)$$

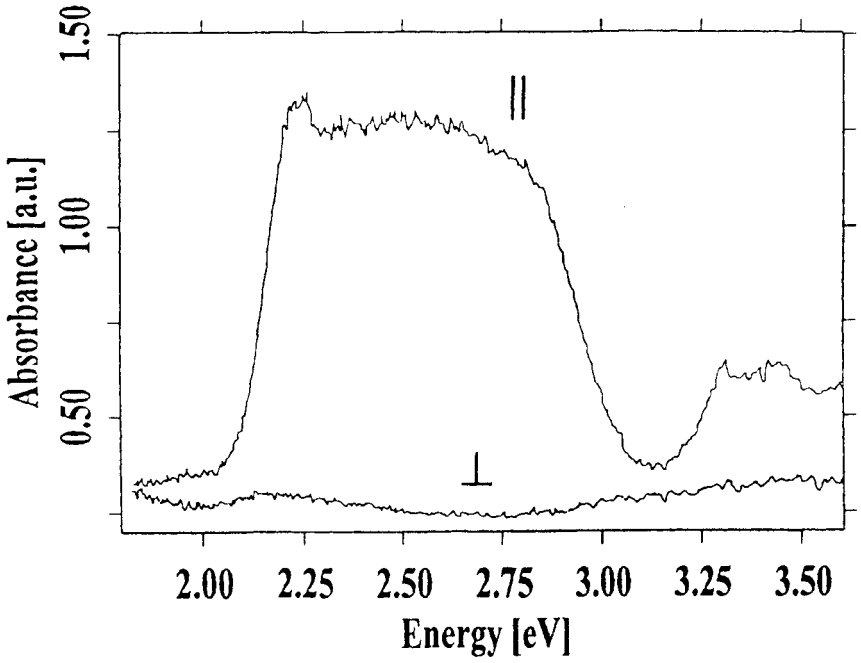


FIGURE 4 Polarized absorption spectrum of PTCDA single crystals at 300 K. Light is polarized in molecular plane in the parallel (||) spectrum and normal to it in the perpendicular (⊥) spectrum; from ref. 6

where $\rho_i$ are atomic charges and eclipsed PTCDAs have $Z_{ij} = R$. The dipole of $|M^-M^+\rangle$ is $-\mu_{CT}$. We add $H' = -\mu_{CT}F_z$ to $H_d$ in (10), thereby breaking inversion symmetry. H′ is diagonal and restricted to r = 3 and 4, with matrix elements

$$\langle r, m'n'|\mu_{CT}F_z|r, mn\rangle = \mp\mu_{CT}F_z\delta_{mm'}\delta_{nn'}. \qquad (17)$$

The solution of $H_d + H'$ goes through as before and yields the EA spectrum in Fig. 5 on subtracting the F = 0 absorption.[6] The calculated $\Delta\alpha_z$ for an isolated dimer is 150 Å$^3$ and depends sensitively on $\Delta$ and $t_e = t_h$. The EA profile also depends on line widths, especially for the 2.5 eV feature in Fig. 5. The profile is in fair agreement with experiment,[34] which has a 20% deeper minimum than the initial maximum and another maximum around 2.45 eV for $F_z$.

Local fields are a major problem for EA fits. Wannier excitons in inorganic crystals are larger than the lattice constant; their Stark shifts are linear in the dielectric constant, $\varepsilon$. The measured PTCDA values along principal axes[35] are $\varepsilon_{zz} = 1.9$ and $\varepsilon_{xx} = \varepsilon_{yy} = 4.5$. This doubles $\Delta\alpha_z$ and agrees well with experiment. But adjacent ions at R are closer than x,y lattice constants and local fields then

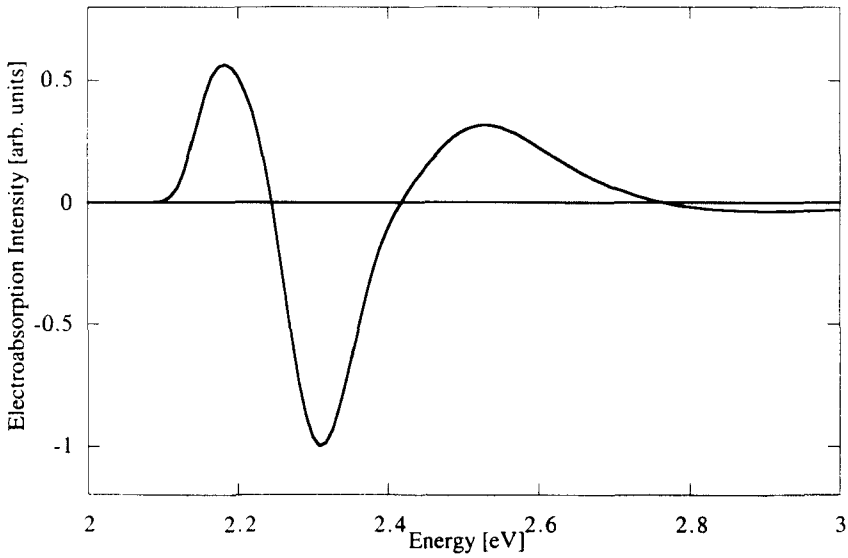


FIGURE 5 Simulated electroabsorption spectra of $H_d$, Eq. (10), for parameters in Table I. The applied field $F_z$ is along the PTCDA stack and shifts the CT states according to Eq. (17)

increase[36] the Stark shift as $\varepsilon^2$. The dielectric properties of molecular solids have been developed in the approximation of self-consistent dipoles.[36,2] PTCDA's carbonyls probably require extensions that are certain to be difficult. Atomic charges for *individual* PTCDA readily improve on point charges or point dipoles, but the self-consistent treatment of a *lattice* in an applied field has not been done and cannot be approximated by a single stack. Although decisive modeling of EA is not yet possible, a Stark shift with F along the stack clearly implicates CT, as recognized by Forrest.[5] The exciton-phonon-CT dimer also accounts for polarized absorption.

PTCDA forms superlattices[5] with layers as thin as 10 ± 5 Å, which corresponds to a stack of three molecules; the other layer is a related conjugated molecule whose $\pi$-$\pi^*$ excitation is above 3 eV. Absorption at 4.2 K is a better resolved version of the 300 K spectrum in Fig. 3b. As shown in Fig. 4–10 of ref. 5, the absorption of 10 and 500 Å films nearly superimpose over the entire range from 1.9 to 3.5 eV. The absence of length dependence, or dispersion, amounts to the dimer approximation introduced above for k = 0 processes.

The Frenkel bandwidth in Fig. 1 is primarily due to dispersion at $k = \pi$, where the Holstein model (2) has in-phase displacements and the overlap $S_\pi$ in (5) exceeds 0.9 for $J \sim \hbar\omega$. The 1–0 emission at 1.71 eV in Fig. 3b dominates, with

weaker n-0 lines whose relative intensities are completely fixed[15] by the variational parameters $\lambda_j$ of Section 3.1. The dispersion is reduced in short stacks with limited delocalization. The lowest excited state of $H_d$, for example, at 2.11 eV is dipole forbidden but gives 1–0 emission at 1.88 eV, including the Stokes shift, with the generation of a ground-state vibration. Weak fluorescence around 1.85–1.90 eV appears in DMSO solutions of PTCDA as a shoulder on the much stronger molecular emission.[37] Using J, g, $\hbar\omega$ and $\delta_S$ in Table I, we find[15] the 1–0 emission of a three-PTCDA stack at 1.82 eV, as observed,[34] which is a 100 meV blue shift relative to the infinite stack. Moreover, 0–0 is weakly allowed in odd-numbered stacks, since the top and bottom of the band are both even, and this accounts for weak emission around 1.95 eV in 10 Å layers.[34]

Singlet exciton motion and Förster transfer are well documented in organic molecular crystals[1,2] and conjugated polymers.[7,8] Four-PTCDA stacks in 10 Å layers are exciton traps that, even in small concentration, can dominate the fluorescence. The photophysics of PTCDA superlattices is still at a preliminary stage and provides tests of other theoretical models. The emission of intermediate layers[34] has a nominal 2–0 feature whose intensity exceeds the 1–0 emission. The molecular 2–0 intensity in Fig. 3a is the upper bound in our model, in which $J > 0$ reduces the vibronic width at the bottom of the Frenkel band. Superlattice emission may consequently require major revisions. Time-resolved and polarized fluorescence provide new applications.

PTCDA has low solubility and aggregates in solution. We recently applied[37] the simple equilibrium, $M + M \leftrightarrow M_2$, to DMSO solutions with total concentration, $c = [M]+[M_2]/2$, ranging from 2.0 to 0.27 μM. The association constant K and monomer concentration [M] are

$$K = [M_2]/[M]^2, \quad [M] = \frac{2c}{1+\sqrt{1+8Kc}}. \tag{18}$$

The integrated fluorescence, due exclusively to monomers, goes as [M] and yields K = 1.85 $\mu M^{-1}$, or 0.34 eV for the dimerization free energy. [M] and $[M_2]$ follow directly from c and K.

The oscillator strength is conserved in exciton theories based on unperturbed molecular states, and Frenkel-CT mixing in excited states retains this feature. The curves in Fig. 6a are solution spectra normalized to equal absorption per PTCDA; the 10 solutions have decreasing c in 20% steps.[37] The isosbestic points, notably at 2.3 eV, confirm an equilibrium between PTCDA and another state that is most likely a dimer. Our model for stacks spreads the $\pi$-$\pi^*(1^1B_u)$ intensity over vibronics with CT character and has equal absorption per PTCDA in solution or stacks, whose profiles are shown in Figs. 3a and b. Taking equal area per PTCDA is simple. Taking dimers in solution to have the film's absorp-

tion is speculative, since there is no structural data in solution, but natural in view of $H_d$. The calculated spectra in Fig. 6b have concentrations [M] and [$M_2$] fixed by (18) and a 40 meV red shift of the entire film spectrum. The striking similarity with experiment supports the equilibrium (18) and the dimer approximation for absorption. A DMSO to solid-state shift of 40 meV hardly matters until baseline corrections are made.

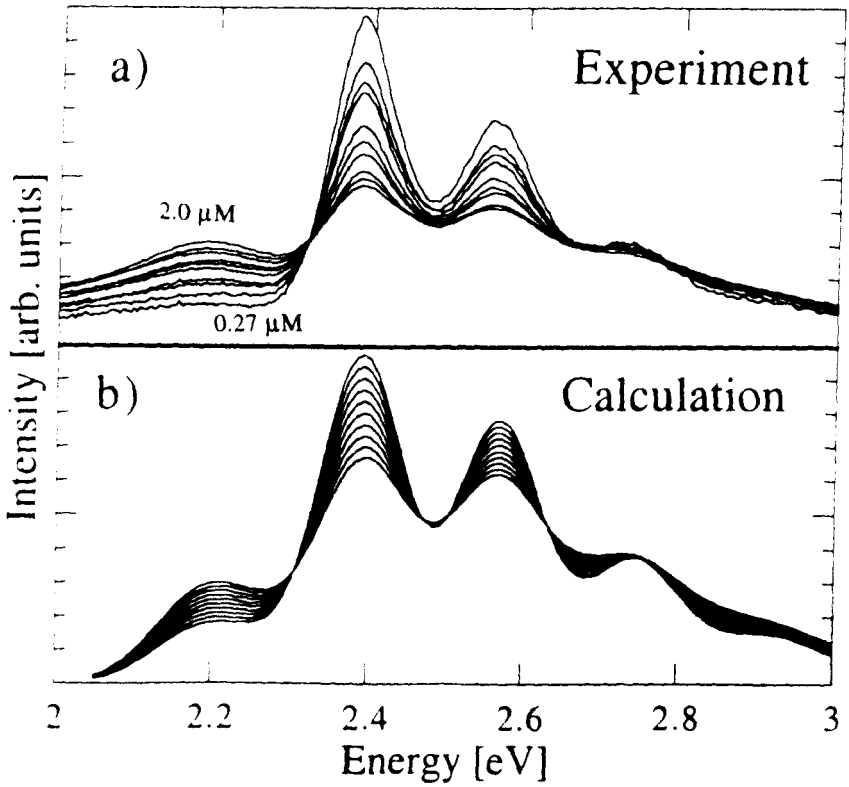


FIGURE 6 (a) PTCDA absorption in DMSO, from ref. 24, normalized to equal areas per molecule; the concentration c decreases from 2.0 to 0.27 μM in 10 dilution steps of 20%; (b) calculated according to the monomer-dimer equilibrium, Eq. (18), and spectra from Fig. 3 for solution and film with equal absorption per molecule

Planar radical ions such as the π-acceptor tetracyanoquinodimethane (TCNQ) and π-donor tetramethyl-p-phenylenediamine (TMPD) also dimerize in solution.[4] They stack face-to-face with < 3.5 Å interplanar separation. Mixed stacks..$D^{+\rho}A^{-\rho}D^{+\rho}A^{-\rho}$.. with partial ionicity ρ are solid-state complexes, while segregated stacks..$D^+D^+D^+$.. or ..$A^-A^-A^-$.. are ion-radical salts with closed-shell

counterions between the stacks. PTCDA exhibits the same behavior for neutral singlets. Monomer-dimer equilibrium is another special feature that extends the scope of theoretical modeling. The 2 μM curve in Fig. 6a has the largest absorption around the 2.23 eV "thumb" of the film and resembles the spectrum in Fig. 3b even more on subtracting the monomer. Most of the solid-state shifts in absorption appear in DMSO, while dimer and superlattice fluorescence shift to lower energy with increasing stack length. Any model must capture these qualitative observations.



## 5. DISCUSSION AND EXTENSIONS

We have emphasized the remarkable structural, electronic and vibrational simplicity of PTCDA: a uniform diatomic chain is an excellent first approximation. Molecular exciton applications to organic crystals have focused on special cases,[1,2] among them crystalline anthracene.[38] Its herring bone structure and vibronics produce extensive changes between solution and crystal spectra that require Davydov splittings; the location of CT states and the conduction edge for generating charge carriers are still under discussion.[4] While PTCDA and related perylenes certainly invite extensions, they have inherent advantages for treating Frenkel and CT excitons. The possibility of direct triplet-exciton generation in anthracene with ruby lasers has produced much information about exciton dynamics and interactions, and the mechanism of carrier generations has been another focus of anthracene studies.[38] Such works are still limited for PTCDA, as are the pump-probe methods used to characterize conjugated polymers.

For detailed investigations, single crystals are obviously preferable to amorphous polymer films. Ordered thin films and control of layer thickness on the molecular level create opportunities that are not possible in single crystals: PTCDA superlattices and sharp interfaces may clarify exciton diffusion or charge generation at the surface. It may be possible to combine comprehensive and detailed experiments with equally complete theory.

Solid-state models range from simple and phenomenological to elaborate and quantitative. We have not considered lattice vibrations that certainly modulate the CT energy $2\Delta$ nor differentiated between PTCDA anion and cation radicals. The present model for mixed Frenkel-CT vibronics emphasizes the minimum requirements, and experimental inputs, of coupling an intramolecular vibration to two nearby electronic excitations. We have discussed stacking contributions to absorption, electroabsorption, fluorescence and fluorescence excitation. The fitting parameters in Table I are consistent with, although different from, the calcu-

lated values in Table II. There are several avenues for improvements or extensions.

The perylene derivatives in Fig. 7 with various substituents R form 18 crystals with one-dimensional stacks.[16] Thin films of $R = CH_3$ (MePTCDI) have recently been studied by Hoffmann et al.[39] at low temperature, where the absorption corresponding to Fig. 3b has four partly-resolved peaks. They mix a Frenkel exciton with three vibronics, p = 0,1 and 2, and a nearest-neighbor CT state with p = 0 to model in-plane and out-of-plane polarization of the four transitions. Frenkel-CT mixing is analogous to (8) and four states allow direct solution of infinite stacks. Vibrational coupling is not treated explicitly, in contrast to the exciton-phonon-CT dimer in Section 3.3. An out-of-plane component for MePTCDI absorption is qualitatively different from the in-plane PTCDA polarization shown in Fig. 4. The MePTCDI stack has larger offsets than PTCDA along the long (x) and short (y) axis from the eclipsed configuration of Fig. 2b. This increases $|M^+M^-\rangle$ mixing with the ground state $|MM\rangle$; such CT mixing is typical in Mulliken complexes and gives out-of-plane polarization.

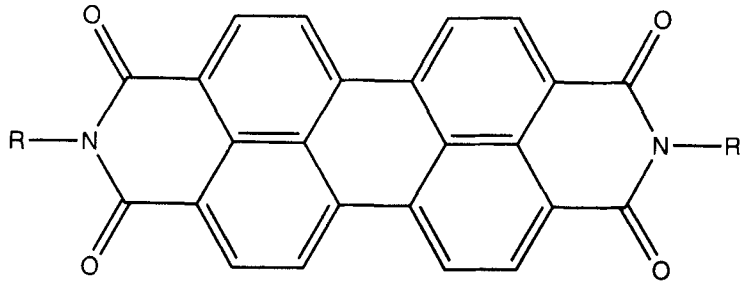


FIGURE 7 Schematic representation of a substituted perylene-3,4:9,10-bis(dicarboximide)

Klebe et al.[16] related the observed $\lambda_{max}$ to x,y offsets of perylene stacks with different R in Fig. 7. While this is less precise because $\lambda_{max}$ refers to the entire spectrum in Fig. 3b, it demonstrates systematic variations due to crystal stacking and illustrates the diversity of perylenes. These stacks offer another test of CT contributions or models. Kazmaier and Hoffmann[40] found HOMO-HOMO and LUMO-LUMO overlaps in dimers as a function of x,y at fixed interplanar separation of 3.5 Å. The overlap splits each frontier orbital. They relate the reduced gap to $\lambda_{max}$, the increased gap from the lower HOMO to upper LUMO to the width of the solid-state spectrum, and find limited agreement with experiment (Fig. 10 of ref. 40).

The overlap interpretation of perylene spectra stands in clear disagreement with molecular exciton theory. First, Frenkel bands are related to hopping inte-

grals J in (14) and transition dipoles (15). Singlet-exciton bands are independent of overlap in the approximation of molecular functions; J is related to the oscillator strength and to Förster transfer with characteristic range up to 50 Å. Second, excitonic absorption is governed by $k = 0$ selection rules and wide bands do not imply broad spectra. Vibronic coupling in Fig. 3 is responsible for the width of PTCDA absorption, while the red-shifted fluorescence of films goes with the bandwidth. It remains to be seen how well molecular excitons account for these perylene stacks.

The sensitivity of PTCDA absorption and EA to the location of the CT states is due to small $t_h$ and $t_e$ in (8). Our fit has a near degeneracy of electronic excitations with several implications. The $k = 0$ gap of $2\Delta \sim \hbar\omega$ is more than doubled at $k = \pi$ for $J \sim \hbar\omega$: weak $k = \pi$ mixing follows on energetic grounds alone. Even within the perylene family, different R in Fig. 7 and x,y offsets change $2\Delta$ and vary CT contributions. HOMO-HOMO and LUMO-LUMO overlaps are required for $t_h$ and $t_e$, respectively. Their calculated values in Table II are based on dimers with R = 3.38 Å and x = 1.19, y = 1.05 Å. The calculated t's have the same sign, which enhances mixing at $k = 0$ and reduces it at $k = \pi$, and $|t_h+t_e|$ is within an encouraging factor of four from the fitted value in Table I. Simulations are insensitive to $t_h \neq t_e$ when $J > t_h, t_e$ because J fixes the linear combinations $|M^*M\rangle \pm |MM^*\rangle$; similarly, variations of $g_+ \neq g_-$ have minor consequences when J is large. These simplifications are unlikely to hold in general for perylene stacks, let alone in molecular crytals with different structures. Frenkel-CT mixing is a general phenomenon that appears as polaron pairs in polymers, but there are many possibilities for vibronic coupling. The most interesting cases of small or negative $\Delta$ are the most sensitive to molecular vibrations.

We presented in Section 4 experimental support for the dimer approximation at $k = 0$. The four-site version of $H_d$ in (10) with cyclic boundary conditions is still tractable numerically.[29] The nonadiabatic basis $|r;mnst\rangle$ has four displaced oscillators and there are 5960 basis states up to $8\hbar\omega$. PTCDA inputs lower the tetramer $E_1$ by 7 meV compared to the dimer; this is negligible at the present resolution. But the effective mass at the top of mixed Frenkel-CT bands depends on model parameters and is not large in general. Tetramer results at $k = \pi$ confirm that CT contributions are small and explicitly give the phonon-assisted absorption at $E_\pi + \hbar\omega$ shown in Figs. 1 and 3b. Its relative intensity is adjustable at present and requires the density of states around $k \sim \pi$ in the Holstein model (2).

As already noted, phonon-assisted absorption in the $k = \pi$ manifold explains the 2.11 eV peak in the fluorescence excitation spectrum.[24] PTCDA absorption is mainly to $k = 0$ states; although rapid, energy transfer or exciton scattering to $k = \pi$ may involve radiationless processes that are bypassed in direct excitation at $k = \pi$. Exciton kinetics is an interesting extension. Energy transfer to the lowest

singlet occurs on the ps time scale in molecules or conjugated polymers,[8] while fluorescence is a ns process. Normal diffusion is a first approximation for weak Frenkel-CT mixing at $k = \pi$. The PTCDA photocurrent closely follows[41] the absorption in Fig. 3b and leads to typical diffusion constants when analyzed conventionally as charge generation at the surface. Simple stacks and low-energy CT may open the way for more quantitative modeling of charge generation.

In summary, we have discussed why PTCDA is particularly suitable for modeling solid-state perturbations of molecular spectra. Molecular stacking in PTCDA and perylenes leads to one-dimensional systems, in contrast to typical organic molecular crystals. Perylene's $\pi$-$\pi^*$ transition is directly related to polyenes and conjugated polymers, with strong coupling to the effective conjugation coordinate and resolved vibronics in solution. The near degeneracy of an adjacent ion pair in the stack with the $\pi$-$\pi^*$ excitation is analogous to a polaron pair on adjacent polymer strands and makes PTCDA an ideal system for modeling interchain interactions. The wealth of PTCDA spectra made possible by thin films and superlattices is remarkable. Much additional information, including time resolved studies, can be expected and will require more comprehensive analysis. The special features emphasized in the present model are Frenkel-CT mixing and coupling to an intramolecular mode, as inferred from PTCDA absorption and fluorescence spectra.



## Acknowledgements

We thank V. Bulovic, S.R. Forrest, D.S. McClure, A. Girlando and Y. Anusooya for stimulating discussions. We gratefully acknowledge support from the National Science Foundation through DMR-9530116, CHE-9707958, and the MRSEC program under DMR-9400362.

## References

1. M. Pope and C.E. Swenberg, *Electronic Processes in Organic Crystals* (Clarendon, Oxford, 1982).
2. E.A. Silinsh and V. Capek, *Organic Molecular Crystals: Interaction, Localization and Transport Phenomena* (Am. Inst. Phys., New York, 1994).
3. P.J. Bounds, W. Siebrand, I. Eisenstein, R.W. Munn and P. Petelenz, *Chem. Phys.* **95**, 197–212 (1985).
4. Z.G. Soos and D.J. Klein, in *Molecular Association*, R. Foster, Ed. (Academic, London, 1975), p. 1–109.
5. S.R. Forrest, *Chem. Rev.* **97**, 1793–1896 (1997) and references therein.
6. M.H. Hennessy, Z.G. Soos, R.A. Pascal, Jr. and A. Girlando, *Chem. Phys.* **245**, 199–212 (1999).
7. T.A. Skotheim, R. Elsenbaumer and T. Allen, Eds. *Handbook of Conducting Polymers, 2nd Ed.* (Marcel Dekker, New York, 1997) and references therein.
8. N.S. Sariciftci, Ed. *Primary Photoexcitations in Conjugated Polymers: Molecular Exciton versus Semincoductor Band Model* (World Scientific, Singapore, 1997) and refereces therein.
9. Z.G. Soos, D. Mukhopadhyay, A. Painelli and A. Girlando, in ref. 7, pp. 165–196.
10. A.J. Heeger, S. Kivelson, J.R. Schrieffer and W.P. Su, *Rev. Mod. Phys.* **60**, 781–850 (1988).

11. E. Conwell, in ref. 8, pp. 99–115.
12. M. Muccini, E. Lunedei, C. Taliani, D. Beljonne, J. Cornil and J.L. Brédas, *J. Chem. Phys.* **109**, 10513–20 (1998).
13. Z.G. Soos, M.H. Hennessy, and G. Wen, *Chem. Phys. Lett.* **274**, 189–95 (1997).
14. M. Gussoni, C. Castiglione and G. Zerbi, in *Advances in Spectroscopy: Spectroscopy of Advanced Materials*, R.J.H. Clark and R.E. Hester, Eds. (Wiley, New York, 1991) pp. 251–353.
15. M.H. Hennessy, R.A. Pascal, Jr. and Z.G. Soos, SPIE Proceedings, Vol. 3797, 89–100 (1999).
16. G. Klebe, F. Graser, E. Hädicke and J. Berndt, *Acta Cryst.* **B45**, 69–77 (1989).
17. A. Camerman and J. Trotter, *Proc. R. Soc. London, Ser. A* **279**, 129–46 (1964).
18. Z.G. Soos and G.W. Hayden in *Electroresponsive Polymeric Systems*,, T.A. Skotheim, Ed. (Marcel Dekker, New York, 1988) pp. 197–266.
19. U. Gomez, M. Leonhardt, H. Port and H.C. Wolf, *Chem. Phys. Lett.* **268**, 1–6 (1997).
20. M.F. Granville, B.E. Kohler and J.B. Snow, *J. Chem. Phys.* **75**, 3765–69 (1981).
21. A. Lovinger, S.R. Forrest, M.L. Kaplan, P.H. Schmidt and T. Venkatesan, *J. Appl. Phys.* **55**, 476–82 (1984).
22. T. Holstein, *Ann. Phys.* **8**, 325–42, 343–89 (1959).
23. D. Feinberg, S. Ciuchi and F. de Pasquale, *Int. J. Mod. Phys.* **B4**, 1317–67 (1990); Y. Toyozawa, in *Organic Molecular Aggregates*, Springer Series in Solid-State Sciences, Vol. 49 P. Reinecker, H. Haken and H.C. Wolf, Eds. (Springer-Verlag, Berlin, 1983) pp. 90–106.
24. V. Bulovic, P.E. Burrows, S.R. Forrest, J.A. Cronin and M.E. Thompson, *Chem. Phys.* **210**, 1–12 (1996).
25. G. Wellein and H. Fehske, *Phys. Rev.* **B56**, 4513–17 (1997).
26. Y. Zhao, D.W. Brown and K. Lindenberg, *J. Chem. Phys.* **106**, 5622–30 (1997); D.W. Brown, K. Lindenberg and Y. Zhao, *J. Chem. Phys.* **107**, 3179 (1997).
27. R.E. Merrifield, *J. Chem. Phys.* **40**, 445–50 (1964).
28. P.O.J. Scherer and S.F. Fischer, *Chem. Phys.* **86**, 269–83 (1984).
29. M.H. Hennessy, PhD Thesis, Princeton University, 2000 (unpublished).
30. W. J. Hehre, L. Radom, P. v. R. Schleyer, and J. A. Pople, *Ab Initio Molecular Orbital Theory*; (John Wiley & Sons, New York, 1986) pp 63–100 and 133–344.
31. A.D. Becke, *J. Chem. Phys.* **98**, 5648–52 (1993); C. Lee, W. Yang, and R. G. Parr, *Phys. Rev.* **B37**, 785–89 (1988); B. Miehlich, A. Savin, H. Stoll, and H. Preuss, *Chem. Phys. Lett.* **157**, 200–206 (1989).
32. G. Wen and Z.G. Soos, "Correlated π-Electronic States: Pyrene, 16-site polyene, and $D_{2h}$ Symmetry Adaptation", *J. Chem. Phys.* **108**, 2486–94 (1998).
33. Z.G. Soos, G.W. Hayden, P.C.M. McWilliams and S. Etemad, *J. Chem. Phys.* **93**, 7439–48 (1990).
34. E.I. Haskal, Z. Shen, P.E. Burrows and S.R. Forrest, *Phys. Rev.* **B51**, 4449–62 (1995).
35. Z. Shen and S.R. Forrest, *Phys. Rev.* **B55**, 10578–92 (1997).
36. D. Fox, *Chem. Phys.* **17**, 273–84 (1976); D. A. Dunmur and R.W. Munn, *Chem. Phys.* **11**, 297–303 (1976).
37. M.H. Hennessy, Z.G. Soos and V. Bulovic, MRS Proceedings, Boston, 1999 (in press).
38. R.G. Kepler in *Treatise on Solid State Chemistry*, Vol. 3, N.B. Hannay, Ed. (Plenum, New York, 1976) p. 615–78.
39. M. Hoffmann, K. Schmidt, T. Fritz, T. Hasche, V.M. Agranovich and K. Leo, *Chem. Phys.* **258**, 73 (2000).
40. P.M. Kazmaier and R. Hoffmann, *J. Am. Chem. Soc.* **116**, 9684–91 (1994).
41. V. Bulovic and S.R. Forrest, *Chem. Phys.* **210**, 13–25 (1996).